Urmia University

Water and Environmental Challenges

2025;1(2):50-57

Journal homepage: https://jwec.urmia.ac.ir

Water & Environmental Challenges

Effect of the Shape and Permeability Percentage of Rigid Spur Dike Nose on the local Scour Depth

Shaghayegh Pourbabak[a]*, Ali Hosseinzadeh Dalir [b], Davoud Farsadizadeh[c]

[a] Ph.D. Candidate in hydraulic structure, Urmia University, Urmia, Iran
[b] Professor, Department of Water Engineering, Tabriz University, Tabriz, Iran
[c] Professor, Department of Water Engineering, Tabriz University, Urmia, Iran

A B S T R A C T

Spur dikes, also known as groynes, are transverse hydraulic structures constructed along riverbanks to protect shores from erosion. By diverting flow away from the bank and concentrating it toward the channel centerline, they improve the hydraulic efficiency of open channels and reduce bank erosion. These structures are commonly installed upstream of bridges. However, spur dikes are highly vulnerable to local scour, especially at the nose (head), due to flow acceleration and vortex formation, which can lead to structural failure. This experimental study examines the effects of nose shape (L-shaped, T-shaped, and straight) and different permeability percentages (0% to fully permeable) on local scour depth around rigid spur dikes under both submerged and unsubmerged flow conditions. Tests were conducted in a laboratory flume with movable bed. Results indicated that all configurations performed better under submerged conditions. Increasing nose and body permeability up to 42.77% significantly reduced scour depth around the body by approximately 35% and at the nose by about 10%. Fully permeable spur dikes showed the best performance in unsubmerged flow, while designs with a rigid body and permeable nose were most effective in submerged conditions. These findings provide practical insights for optimizing spur dike design to minimize scour and enhance stability.

Keywords:
local scour
spur dike
permeable spur dike
compound spur dike
nose geometry

1. Introduction

Rivers have long been central to human civilization, with many major cities established along their banks. River engineering addresses critical challenges such as bank erosion, sedimentation, flood control, and channel stabilization. Spur dikes, also known as groynes, are transverse structures that extend from the riverbank into the flow. They protect banks by redirecting streamlines toward the channel centerline and are commonly installed upstream of bridges. Local scour depth, resulting from concentrated flow acceleration and vortex formation around the spur dike nose, often exceeds general scour and poses a major threat to the stability of these structures. Accurate prediction and mitigation of local scour are therefore essential for the design of stable river training works. Recent guidelines recommend that impermeable spur dikes should not exceed 15% of the channel width, while permeable designs can extend up to 25% due to lower flow blockage and reduced turbulence (Lagasse et al., 2021).

* Corresponding authors.
E-mail address: sh.pourbabak@urmia.ac.ir
https://doi.org/ 10.30466/jwec.2026.56684.1009
Received: 22 October 2025
Accepted: 18 May 2026

Numerous studies have examined scour around spur dikes and the influencing factors. Dey and Das (2018) reviewed scour dynamics around impermeable spur dikes in straight and curved channels, highlighting vortex formation and recommending that spur dike length should be limited to less than half the floodplain width to reduce scour and flood risks. Amini et al. (2012) conducted laboratory tests on permeable and impermeable spur dikes and found that scour depth is proportional to discharge and inter-dike spacing, with permeable designs generating higher bed turbulence. Karimaee Tabrizi and Kashefipour (2020) observed increased Reynolds stress along the dike axis but 20–30% lower sediment concentrations due to lateral deposition in permeable spur dikes — a feature absent in impermeable ones.

Mehrain et al. (2014) analyzed flow structures near straight spur dikes and reported that maximum velocities and turbulent parameters occur adjacent to the dike, with peak scour at approximately 45° downstream due to horseshoe vortex intensification. Sukhodolov et al. (2023) confirmed these findings through three-dimensional numerical simulations. Amini et al. (2015) and Pandey et al. (2022) demonstrated a direct relationship between scour depth and the Froude number, noting that submerged conditions can reduce equilibrium scour depth by up to 18% in permeable designs.

Yabarpour and Kashefipour (2014) showed that Froude numbers greater than 0.3 significantly increase scour hole dimensions around impermeable spur dikes. Ezzeldin and Abdelrazek (2019) reported that permeability exceeding 40% can reduce scour depth by 35–50% through seepage and flow diffusion. Regarding geometry, Abbasi and Maleknejad (2013) and Wang et al. (2024) indicated that T-shaped and L-shaped spur dikes can notably influence scour patterns, with optimized shapes providing up to 22% reduction in tip scour.

While prior research has addressed spur dike geometry and permeability separately, few studies have investigated the combined effects of nose shape and permeability percentage — particularly nose-specific permeability — under both submerged and unsubmerged conditions. This important gap has been highlighted in recent reviews (Wang et al., 2024; Zhang and Nakagawa, 2025). The present study aims to address this gap through laboratory experiments that quantify the effects of three nose shapes (L-shaped, T-shaped, and straight hexagonal) and different permeability percentages on local scour depth at both the nose and body of spur dikes.

2. Materials and Methods

2.2. Dimensional Analysis

To relate factors influencing scour around spur dikes, dimensional analysis was applied to key parameters:

$$f1(\rho, V, H, B, L_x, H_{SD}, \alpha, g, D_{50}, \rho_s, Vc, Q, A, \mu, H)=0 \quad (1)$$

where ρ is the fluid density, V is approach velocity, H is flow depth, B is channel width, L_x is spur dike length, figure (1), H_{SD} is dike height, α is permeability ratio, g is gravity, D_{50} is median bed particle diameter, ρ_s is sediment density, V_c is critical velocity, Q is discharge, A is cross-sectional area, μ is dynamic viscosity, and H_S is nose scour depth.

Figure 1. Geometric parameters of the spur dike

By Buckingham π theorem:

$$\frac{H_s}{H} = f_2\left(\frac{L_x}{H}, \frac{V_C}{V}, \frac{gH}{V^2}, \frac{Q}{VH^2}, \frac{B}{H}, \frac{H_{SD}}{H}, \alpha, \frac{D_{50}}{H}, \frac{\rho_S}{\rho}, \frac{\mu}{\rho VH}, \frac{A}{H^2}\right) \quad (2)$$

Considering that the variables B, L_x, D_{50}, ρ_s, ρ are constant values in all the experiments, the conditions of clear water $\left(\frac{V_C}{V} \leq 0/95\right)$ prevail during the experiments, and also by considering the flow rate, speed and depth of the flow constant, it can be obtained from the dimensionless parameters $\frac{V_C}{V}, \frac{\rho_s}{\rho}, \frac{B}{H}, \frac{Q}{VH^2}, \frac{l_x}{H}, \frac{D_{50}}{H}$ ignored With these simplifications, the following relationship is obtained:

$$\frac{H_s}{H} = f_3\left(\frac{H_{SD}}{H}, Fr, R_e, \alpha, \frac{A}{H^2}\right) \quad (3)$$

In relation (3), the flow velocity remains unchanged, and the Froude number and Reynolds number are also omitted. Thus, the final relation can be expressed as:

$$\frac{H_s}{H} = f_4\left(\frac{H_{SD}}{H}, \alpha, \frac{A}{H^2}\right) \quad (4)$$

In this regard, if $\frac{H_{SD}}{H}$ >1 is the condition of non-submerged flow and if it is $\frac{H_{SD}}{H}$<1, the condition of the flow will be submerged.

2.2. Laboratory Equipment

Experiments occurred in a 6 m long, 0.8 m wide, 0.5 m high glass-walled rectangular flume at the University of Tabriz Hydraulic Laboratory. Bed slope ranged from 0 to 0.03%, with a downstream stilling basin and rectangular weir for discharge measurement. A 100-hp pump supplied up to 60 L/s from a reservoir, regulated by a downstream valve. Tailgates and a butterfly valve controlled depth. Post-flume, water passed a debris screen into a sump.

Spur dike models had a 35 cm height, 14cm total length (12 cm body, 2 cm nose width), and rectangular cross-section of wood and stone mesh. Three nose shapes were tested: T-shaped (14 cm), L-shaped (6 cm), and straight (hexagonal, 8 cm). Five series (six tests each) varied permeability: (1) fully rigid (submerged/unsubmerged); (2) fully permeable; (3) rigid body, fully permeable nose; (4) rigid body, 42.77% permeable nose; (5) 42.77% permeable body and nose. Figure (2).

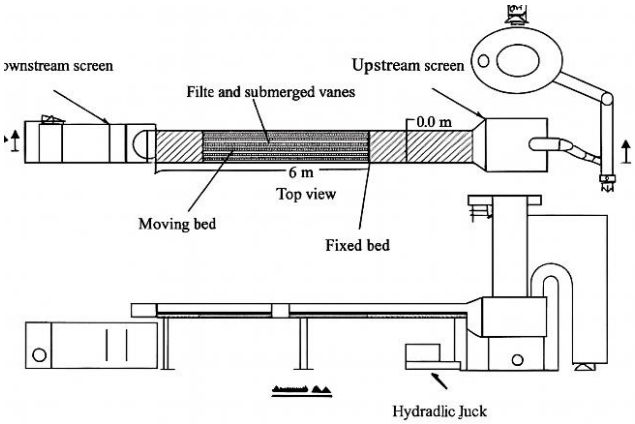

Figure 2. Overview of the laboratory flume

2.3. Experimental Procedure

Spur dikes were installed mid-flume against the right wall on a leveled sand bed. Tests ran at 21 cm depth (submerged, 38.745 L/s) and 16 cm depth (unsubmerged, 29.778 L/s), yielding $y/L > 1$ (1.14–1.5) and $V/V_c =$ 0.9for clear-water conditions. Flow stabilized for 3.5 hours, followed by 9-hour runs to equilibrium. Scour depths were measured at nose and body; bed topography was profiled post-drainage (Fig. 3). Flow initiated gradually via upstream valve, with downstream flap gate adjusting to near-weir overflow, figure (3).

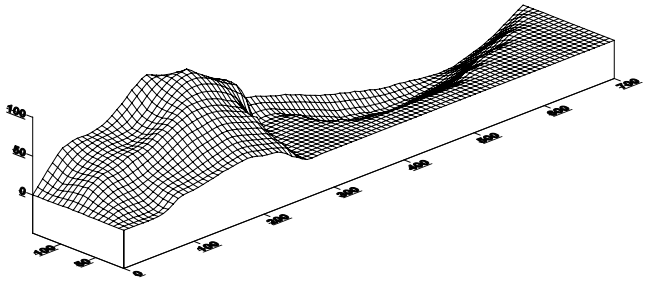

Figure 3.Contour map of bed elevation showing the scour hole and downstream depositional ridge around spur dike B4

2.4. Physical model of the spur dike

The spur dike models feature a fixed rectangular cross-section constructed from wood and stone mesh, measuring 35 cm in height and 14 cm in total length. The body of the spur dike is 12 cm long, while the nose width is 2 cm. Three different nose designs were created: a T-shaped nose measuring 14 cm, an L-shaped nose measuring 6 cm, and a hexagonal nose measuring 8 cm. The experiments were conducted in five series, each consisting of six tests. In the first series, all models had rigid bodies and noses in both submerged and non-submerged states. The second series employed fully permeable models. The third series featured a rigid body with a fully permeable nose. The fourth series had a fully rigid body paired with a semi-permeable nose. Finally, the last series included models with semi-permeable bodies and noses. A sample of the rigid T-shaped spur dike model is illustrated below, Figure (4).

Figure 4.A view of the final scour profile in a T-shaped all-rigid spur dike

2.5. Discharge Measurements

The flow selected in the experiments was measured with the rectangular overflow at the end of the channel and through the following relationship:

$$Q(m^3/s) = 1.708(0.6 - 0.2h)h^{1.5} \qquad (5)$$

where h is the water upstream of the overflow in meters. Discharge measurements were obtained using a rectangular spur dike, with flow profiles recorded manually by a calibrated staff gauge and a graduated tank installed at the end of the channel. The instruments were calibrated against standard volumetric measurements, and the calculated values are based on the standard rectangular spur dike equation, ensuring reliability within the typical accuracy range of hydraulic laboratory practice.

The flow rate was obtained according to the y/L ratio in such a way that the water depth should be greater than the effective length of the structure (y/L>1). which was calculated according to the length of the spur dike, the depth of the flow, the speed of the flow, and the geometry of the (rectangular) section of the flow. The flow speed was adjusted by the dams in such a way that sediment transport does not happen downstream. In the laboratory, it was worked with two flow rates: 38.745 liters per second for the submerged state and 29.778 liters per second for the non-submerged state. The discharges selected for the experiments—38.745 L/s in submerged conditions and 29.778 L/s in non-submerged conditions—were determined to maintain a hydraulic regime where the ratio of flow depth to spur dike length (y/L) exceeded unity. This ensured that the flow depth was greater than the effective length of the spur dike (14 cm), thereby isolating the influence of spur dike nose geometry and permeability on local scour without introducing variability related to insufficient depth.

The corresponding flow depths of 21 cm (submerged) and 16 cm (non-submerged) yielded y/L ratios between 1.143 and 1.5, which lie within the recommended range for minimizing depth-induced effects on scour formation. Flow velocities were further adjusted to achieve V/Vc = 0.9, thereby maintaining clear-water conditions and preventing sediment transport downstream. This experimental setup provided a controlled environment for comparing different spur dike geometries and permeability percentages, while ensuring consistency in sediment entrainment and flow structure.

In the first experiment, the L-shaped spur dike with a body length of 12 cm and a nose of 6 cm in non-submerged conditions with a completely rigid body and nose in a vertical position in clear water conditions with V/Vc=0.9 and with the aim of determining the maximum amount of scour depth, especially around the nose and its effect on the body, as well as recording the time changes of the scouring cavity were used.

In table (1), the introduction of spur dikes has been discussed.

Table 1. Types of spur dikes studied in this research

Name	Permeability percentage (non-submerged)	shape of the spur dike	Row	Name	Permeability percentage (submerged)	shape of the spur dike	Row
A6	Completely rigid	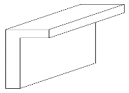	2	A1	Completely rigid	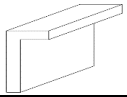	1
A7	Completely permeable	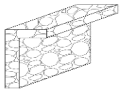	4	A2	Completely permeable		3
A8	The body is completely rigid; the nose is completely permeable	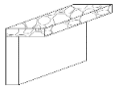	6	A3	The body is completely rigid; the nose is completely permeable	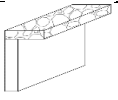	5

A9	The body is completely rigid and the nose is 42.77% permeable	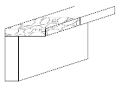	8	A4	The body is completely rigid and the nose is 42.77% permeable	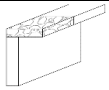	7
A10	Body and nose 42.77% permeable	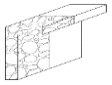	10	A5	Body and nose 42.77% permeable	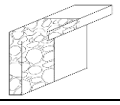	9
B6	Completely rigid	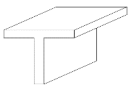	12	B1	Completely rigid	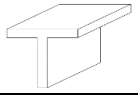	11
B7	Completely permeable	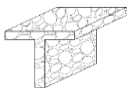	14	B2	Completely permeable	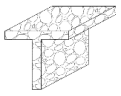	13
B8	The body is completely rigid; the nose is completely permeable	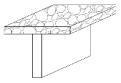	16	B3	The body is completely rigid; the nose is completely permeable	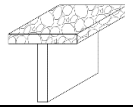	15
B9	The body is completely rigid and the nose is 42.77% permeable	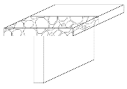	18	B4	The body is completely rigid and the nose is 42.77% permeable	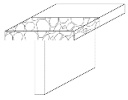	17
B10	Body and nose 42.77% permeable	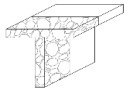	20	B5	Body and nose 42.77% permeable	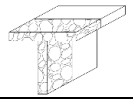	19
C6	Completely rigid	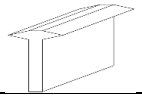	22	C1	Completely rigid	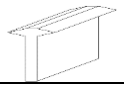	21
C7	Completely permeable	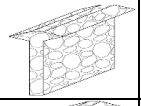	24	C2	Completely permeable	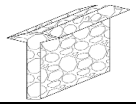	23
C8	The body is completely rigid; the nose is completely permeable	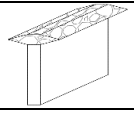	26	C3	The body is completely rigid; the nose is completely permeable		25
C9	The body is completely rigid and the nose is 42.77% permeable	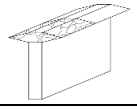	28	C4	The body is completely rigid and the nose is 42.77% permeable	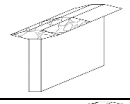	27
C10	Body and nose 42.77% permeable	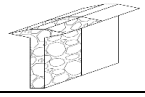	30	C5	Body and nose 42.77% permeable	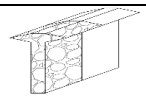	29

3. Results and Discussion

3.1. Flow Pattern and Scour Development

At the beginning of each test, once the discharge (water level) reached the predetermined amount, the flow lines around the spur dike became visible at the water surface. After separating from the nose, these streamlines were directed toward the center of the channel. Sediment scouring initially started at the nose (cape) and gradually extended toward the shore. Approximately 15 minutes later, this scouring spread to the body of the spur dike. Eventually, a small depositional ridge formed on the downstream side of the spur dike, reaching a maximum height of about 1.5 cm. This ridge persisted for a short time (approximately 5 minutes) before being gradually eroded, as shown in Figure 5.

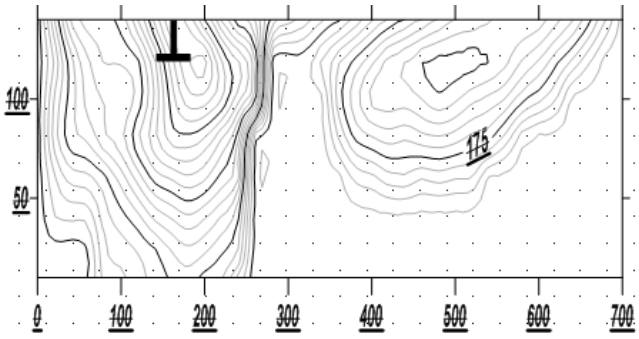

Figure 5. Two-dimensional parallel curves around spur dike B

During all the tests, the total length of the models was constant at 14 cm, and the bed material properties inside the permeable spur dikes remained unchanged. Therefore, these parameters had no influence on the relative comparison of scour depths.

3.2. Effect of Permeability Percentage

Spur dikes with a rigid body and fully permeable nose provided the best (lowest) scour conditions in the submerged state, while fully permeable spur dikes performed best in the non-submerged state. Conversely, the highest scour depths in both submerged and unsubmerged conditions were observed in fully rigid spur dikes.

Figure 6 shows the differences in scour depth for various permeability percentages across the three nose shapes.

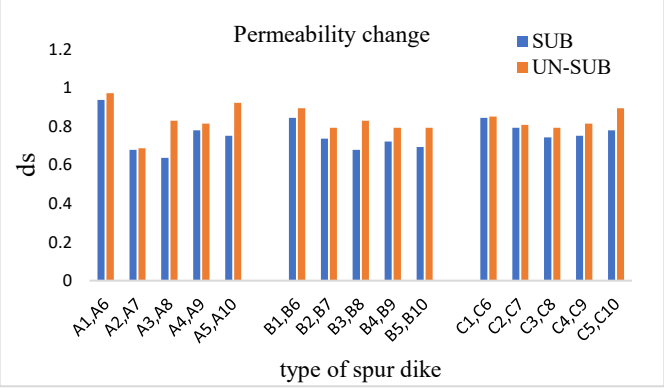

Figure 6. Comparison of differences in permeability percentage in spur dikes

3.3 Effect of Submergence and Nose Geometry on Nose Scour

The experiments were conducted with two different flow conditions: submerged (water depth = 21 cm, Q = 38.745 L/s) and unsubmerged (water depth = 16 cm, Q = 29.778 L/s).

As shown in Figure 7, submerged conditions reduced the nose scour depth by approximately 10% on average compared to unsubmerged conditions. The greatest reduction was observed in spur dike A4 (L-shaped nose with rigid body and 42.77% permeable nose). Among the three geometries, the L-shaped nose generally showed better performance (lower scour) than T-shaped and hexagonal (straight) noses in submerged conditions.

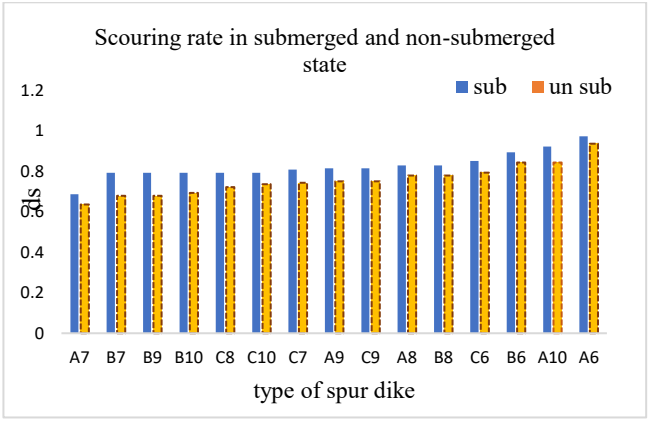

Figure 7.Comparison of the scouring rate at the nose of spur dikes in submerged and unsubmerged conditions (blue: unsubmerged, yellow: submerged)

3.4. Effect of Submergence and Permeability on Body Scour

The beneficial effect of permeability and submergence is much more pronounced on the body of the spur dikes. As illustrated in Figure 8, the combination of submerged conditions and increased permeability reduced body scour by approximately 35% on average. The best performance belonged to spur dike A5 (L-shaped with 42.77% permeable body and nose). Once again, L-shaped configurations demonstrated superior performance in reducing body scour compared to T-shaped and hexagonal noses.

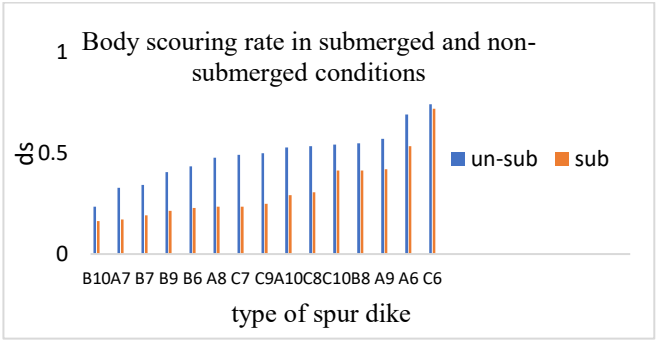

Figure 8.The effect of the permeability percentage and submergence on the amount of scour at the body of spur dikes

3.5 Summary of Key Findings

Increasing the permeability of the nose and body up to 42.77% significantly reduced local scour, with the most notable reduction occurring around the body (about 35%) and a smaller reduction at the nose (around 10%). Submerged conditions consistently performed better than unsubmerged conditions across all configurations. The L-shaped nose combined with partial permeability (42.77%) delivered the best overall performance under submerged flow. Moreover, rigid-body designs with permeable noses were most effective in submerged conditions, while fully permeable designs were

more suitable for unsubmerged conditions. These findings highlight the important synergistic influence of nose geometry and permeability percentage in mitigating local scour around spur dikes. Overall, the results emphasize that optimizing both geometric design and permeability distribution can significantly enhance hydraulic performance and reduce sediment-related risks. This integrated approach can guide the development of more efficient and resilient spur dike structures in river engineering applications.

Conclusion

This study investigated the combined effects of nose shape (L-shaped, T-shaped, and straight hexagonal) and permeability percentage on local scour depth around spur dikes under both submerged and unsubmerged flow conditions. The experimental results clearly demonstrate that nose geometry and permeability interact significantly to reduce local scour, with the most pronounced improvements observed under submerged conditions where flow velocity near the structure is effectively reduced.

Key findings indicate that increasing the permeability of both the nose and body to 42.77% reduced scour depth around the body by approximately 35% and at the nose by about 10% compared to fully rigid configurations. Among the tested geometries, the L-shaped nose consistently exhibited the lowest scour depths in submerged conditions, outperforming T-shaped and hexagonal designs. Overall, designs with a rigid body and permeable nose performed best in submerged flow, while fully permeable spur dikes were most effective in unsubmerged conditions.

These findings highlight the practical importance of integrating optimal nose geometry with appropriate permeability in spur dike design. By adopting such configurations, engineers can substantially mitigate local scour and enhance the long-term stability and performance of riverbank protection structures.

Nevertheless, the present experiments were conducted under controlled laboratory conditions with uniform sediment and steady flow. Natural rivers involve more complex phenomena, including heterogeneous bed materials, unsteady hydrographs, and varying channel geometries. Therefore, further field investigations and numerical studies are recommended to validate and extend these results under real-world conditions.

In conclusion, the synergistic interaction between spur dike nose geometry and permeability percentage offers a promising and effective approach for reducing local scour and improving the resilience of hydraulic structures in river engineering.

References

1. Abbasi, A. A., & Maleknejad, M. (2013). Experimental study of the impact of direct permeable spur dike parameters and the T-shaped on the scouring around them. *Proceedings of the Iranian Society of Irrigation and Drainage*, 43(2), 215-225.
2. Amini, A., Melville, B. W., Ali, T. M., & Ghazvinizadeh, S. (2012). The effects of groin geometry on flow and scour pattern. *Journal of Hydraulic Research*, 50(4), 404-415. https://doi.org/10.1080/00221686.2012.686619
3. Amini, A., Moghadam, M. K., & Solaimani, K. (2015). Effect of relative distance and angle of spur dikes on scour depth. *International Journal of Engineering, Transactions B: Applications*, 28(11), 1651-1658. https://doi.org/10.5829/idosi.ije.2015.28.11b.09
4. Dey, S., & Das, A. (2018). Scour around impermeable spur dikes: A review. *ISH Journal of Hydraulic Engineering*, 24(1), 1-17. https://doi.org/10.1080/09715010.2017.1342571
5. Ezzeldin, R. M., & Abdelrazek, A. M. (2019). Numerical and experimental investigation for the effect of permeability of spur dikes on local scour. *Ain Shams Engineering Journal*, 10(4), 779-790. https://doi.org/10.1016/j.asej.2019.01.001
6. Karimaee Tabrizi, E., & Kashefipour, S. M. (2020). Experimental investigation of suspended sediment transport in channels with permeable spur dikes. *Journal of Hydro-environment Research*, 30, 1-12. https://doi.org/10.1016/j.jher.2020.03.002
7. Lagasse, P. F., Zevenbergen, L. W., Schall, J. D., Clopper, P. E., & Thomson, W. A. (2021). *Stream stability at highway structures* (4th ed.). Federal Highway Administration.
8. Mehrain, M., Rajaratnam, N., & Katopodis, C. (2014). Local scour effects on flow structures near straight spur dikes. *Environmental Fluid Mechanics*, 14(3), 567-589. https://doi.org/10.1007/s10652-013-9315-4
9. Pandey, M., Sharma, P. K., Ahmad, Z., & Kumar, P. (2022). Estimation of maximum scour depth and scour pattern around submerged spur dike. *Proceedings of the 13th International Symposium on River Sedimentation*, 49, 1-10.
10. Sukhodolov, A. N., Ujma, J., Chlewicki, W., & Hildebrandt, A. (2023). Three-dimensional flow structures near straight spur dikes in uniform flow. *Journal of Hydraulic Engineering*, 149(5), 04023012. https://doi.org/10.1061/JHYEFF.HYENG-7890
11. Wang, Y., Li, S., & Zhang, Q. (2024). Experimental study on the optimal spur dike shape under varying

flows for scour reduction. *International Journal of Sediment Research*, 39(2), 200-215. https://doi.org/10.1016/j.ijsrc.2023.10.003

12. Yabarpour, M., & Kashefipour, S. M. (2014). Effect of Froude number on scour hole dimensions around impermeable spur dikes. *Journal of Civil & Environmental Engineering*, 4(3), 1-7. https://doi.org/10.4172/2165-784X.1000142
13. Zhang, H., & Nakagawa, H. (2025). Scour around spur dikes: Recent advances and future research directions in permeable designs. *Annuals of Disaster Prevention Research Institute, Kyoto University*, 68(A), 45-60.